



A new method for the generation of realistic atomistic models of siliceous MCM-41



Christopher D. Williams^{a, b}, Karl P. Travis^{a, *}, Neil A. Burton^b, John H. Harding^a

^a Immobilisation Science Laboratory, Department of Materials Science and Engineering, University of Sheffield, Sheffield, S1 3JD, UK

^b School of Chemistry, University of Manchester, Manchester, M13 9PL, UK

ARTICLE INFO

Article history:

Received 24 December 2015

Received in revised form

5 March 2016

Accepted 22 March 2016

Available online 28 March 2016

Keywords:

MCM-41

Adsorption isotherms

Isosteric heat of adsorption

Henry law constant

Low pressure adsorption

Physisorption

ABSTRACT

A new method is outlined for constructing realistic models of the mesoporous amorphous silica adsorbent, MCM-41. The procedure uses the melt-quench molecular dynamics technique. Previous methods are either computationally expensive or overly simplified, missing key details necessary for agreement with experimental data. Our approach enables a whole family of models spanning a range of pore widths and wall thicknesses to be efficiently developed and yet sophisticated enough to allow functionalisation of the surface – necessary for modelling systems such as self-assembled monolayers on mesoporous supports (SAMMS), used in nuclear effluent clean-up.

The models were validated in two ways. The first method involved the construction of adsorption isotherms from grand canonical Monte Carlo simulations, which were in line with experimental data. The second method involved computing isosteric heats at zero coverage and Henry law coefficients for small adsorbate molecules. The values obtained for carbon dioxide gave good agreement with experimental values.

We use the new method to explore the effect of increasing the preparation quench rate, pore diameter and wall thickness on low pressure adsorption. Our results show that tailoring a material to have a narrow pore diameter can enhance the physisorption of gas species to MCM-41 at low pressure.

© 2016 The Authors. Published by Elsevier Inc. This is an open access article under the CC BY license (<http://creativecommons.org/licenses/by/4.0/>).

1. Introduction

Ever since it was first synthesized by Mobil, in 1992 [1,2], MCM-41, a silica-based porous material, has attracted widespread interest from both industry and the academic community. MCM-41 contains well-defined cylindrical pores arranged in a hexagonal configuration. These pores have diameters that typically vary from 1.5 to 10 nm [1,3–7], classifying MCM-41 as a mesoporous material. The high surface area, large pore volume and exceptional hydrothermal stability [8,9] make MCM-41 an excellent choice as an industrial adsorbent. The synthesis, based on a liquid-crystal templating mechanism, enables tight control over the pore size distribution. MCM-41 can be made with different pore-wall thicknesses, varying between 0.6 and 2 nm [7,8], and a wide range of silanol densities [10–13], depending on the exact conditions of synthesis. The ease of functionalisation of the mesopores allows

enhancement in selectivity and specificity, offering a significant advantage over competing porous materials. Applications include gas separation [14], catalysis [15] and environmental remediation [16]. The potential of MCM-41 as an effective material for difficult separation problems has been recognized, especially in the case of CO₂ removal from gas mixtures where the selectivity and adsorbent capacity of zeolites and activated carbons can be poor in the high temperature conditions encountered in flue gas streams [17].

Molecular simulation offers the ability to rapidly screen large sets of candidate materials with different pore diameters, wall thicknesses and surface chemistries, to find those with the most promising selectivity for experimental synthesis, with obvious cost-savings. Key to this process is the ability to construct accurate atomic models of MCM-41. Although the structure of MCM-41 is well known at the mesoscale, there is less certainty over its exact structure at the nanoscale. Uncertainty remains over the thickness of the pore walls, whether these walls are completely amorphous or partially crystalline, and the presence of surface irregularities and micropores. This has led to a plethora of models being proposed for MCM-41, displaying a wide variety of complexity.

* Corresponding author.

E-mail address: k.travis@sheffield.ac.uk (K.P. Travis).

The first attempt at constructing an atomistic model of MCM-41 consisted of defining cylinders of frozen atoms ('micelles') in the simulation box and then either randomly placing silicon and oxygen atoms in the gaps between them, or alternatively, placing cylindrical sheets of SiO₂ around them, followed by structural relaxation using molecular dynamics (MD) [18].

Maddox and Gubbins constructed a simplified model that consisted only of oxygen atoms from which they derived a smooth, one-dimensional potential energy function, dependent only on the radial distance from the pore surface [19]. Their potential was obtained by integrating over the oxygen atoms in a manner similar to that used to construct the so-called 10-4-3 potential for carbon slit-pores [20]. Using this model they obtained simulated adsorption isotherms using argon and nitrogen as adsorbates. Agreement with experimental isotherms was generally poor in the low pressure region but this was improved upon by introducing surface heterogeneity; an explicit atom MCM-41 was used which was then divided into 8 sectors, each with a different solid–fluid interaction energy [21].

Klestorfer et al. carved pores from a lattice of α -quartz, saturating the surface with hydroxyl groups followed by relaxation of the structure using MD [22]. They determined that the most stable MCM-41 structures had pore diameters ranging from 3.5 to 5 nm and wall thicknesses between 0.8 and 1.2 nm.

He and Seaton [23] studied three models of increasing complexity. Model 1 comprised concentric cylinders of oxygen atoms arranged in a regular array, model 2 was constructed from cutting cylindrical holes from a block of α -quartz while model 3 was an amorphous structure created using a stochastic scheme. Only the latter model was able to accurately reproduce the experimental adsorption isotherm for CO₂. The two simplified models, in which the surface was either homogeneous or completely crystalline, underestimated the amount of adsorption, including in the low pressure region of the isotherm.

More recently, various workers have constructed MCM-41 models by simulating the actual self-assembly process of micelles [24–26], even incorporating the silanol condensation process [27]. There have been numerous other attempts to build atomistic models of MCM-41 and these have previously been reviewed and compared [28].

For many of the possible applications of MCM-41, it is necessary to include a realistic atomistic configuration of the pore surface, decorated with silanol groups, to enable surface functionalisation and the possibility of deprotonation in aqueous solution. Therefore, many of the models discussed are too simplistic in their level of detail of the MCM-41 surface. Of those that do include sufficient detail, significant computational resource is required to construct just a single model. There is, therefore, a need for a new and efficient method of preparing models of MCM-41 in such a way that easily allows for the structural parameters (such as pore diameters and wall thicknesses) of the material to be optimised. We present such a model in this publication.

Our approach to building the MCM-41 models (using a modified Buckingham potential and a MD melt-quench routine) enables pore diameters and wall thicknesses to be tuned so as to enhance adsorption. The models were validated by computing the CO₂ adsorption isotherm using grand canonical Monte Carlo (GCMC) simulations and compared to experiment. A simple Monte Carlo scheme was used to investigate the effect of pore diameter and wall thickness on the adsorption behaviour of simple gases at very low pressure. Four gas adsorbates were studied; two with a quadrupole moment (CO₂ and N₂) that are highly sensitive to the charge distribution of the surface, and two that are not (Ar and Kr).

2. Methodology

2.1. Preparation of MCM-41 using melt-quench MD

Our method for constructing models of MCM-41 comprises three main steps. The first step makes an amorphous solid silica structure, while the second step removes atoms to create the pore space and the third, and final step, modifies the surface chemistry. Common to all three steps is the use of the molecular dynamics (MD) simulation method. MD solves Newton's equations of motion using a finite difference approximation to generate time ordered sets of positions and momenta which, when combined with the ideas of Boltzmann's statistical mechanics, yields thermodynamic properties that can be compared with experiment for a sufficiently large number of atoms. The key ingredient in any MD simulation is the interaction potential, from which expressions for the Newtonian forces can be derived.

For interactions between Si and O atoms, the following modified Buckingham pair potential, ϕ_B , was employed:

$$\phi_B(r_{ij}) = \frac{q_i q_j}{4\pi\epsilon_0 r_{ij}} + A_{ij} \exp(-B_{ij} r_{ij}) - \frac{C_{ij}}{r_{ij}^6} + \frac{D_{ij}}{r_{ij}^{12}} - \frac{E_{ij}}{r_{ij}^8} \quad (1)$$

where q_i is the partial charge of atom i , ϵ_0 is the vacuum permittivity and r_{ij} is the distance between atoms i and j . The coefficients A_{ij} , B_{ij} , C_{ij} are the parameters for each interacting pair of atoms, originally derived from *ab initio* calculations of silica clusters [29]. D_{ij} , is an additional repulsive term included to avoid the unphysical fusing of atoms at high temperatures caused by the attractive divergence of the Buckingham potential [30] and E_{ij} can be ascribed to the second term in the dispersion expansion [31]. The parameters for each interacting pair are given in Table 1 while the O and Si partial charges were $-1.2e$ and $+2.4e$, respectively.

An initial configuration was prepared by taking a cubic simulation cell containing atoms from an α -quartz crystalline arrangement, ensuring that stoichiometric quantities of Si and O were selected. The total number of atoms ranged from 7290 to 27789, depending on the size of the model.

For each model, the initial configuration was melted in the NPT ensemble at 1 atm by heating to 7300 K at a rate of 100 K ps⁻¹ from room temperature before quenching to 300 K at a controlled rate. These simulations were carried out using the DL_POLY Classic software package. The equations of motion were integrated using the Verlet leapfrog integration algorithm [32] with a 1 fs time step. The short-range part of the interaction potential was spherically truncated at 10 Å and electrostatic interactions were evaluated using the Ewald summation method to a precision of 10⁻⁶ kJ mol⁻¹. Cubic periodic boundary conditions were employed to model the bulk material. Temperature and pressure were controlled using the Nosé-Hoover thermostat and barostat with relaxation times of 0.1 ps. [33,34]. The quench rates investigated ranged from 7000 to 1 K ps⁻¹. The final part of step one was to confirm the presence of an amorphous silica solid. This was achieved by examining isotropic (radial) pair distribution functions calculated over 100 ps duration MD runs and observing the absence of any long range order.

Step two in the construction process makes a porous silica substrate from an initially cubic simulation cell of the amorphous

Table 1
Parameters used in the preparation of MCM-41 models [29,31].

	A_{ij} (eV)	B_{ij} (Å ⁻¹)	C_{ij} (eV Å ⁶)	D_{ij} (eV Å ¹²)	E_{ij} (eV Å ⁸)
O–O	1388.7730	2.7600	175.0000	180.0000	24.0000
Si–O	18003.7572	4.8732	133.5381	20.0000	6.0000

silica. This was achieved by deleting all of the atoms within a chosen pore radius from the quenched silica configuration (Fig. 1a). That is, the coordinates of the set of deleted atoms are given by

$$\{(x, y, z) \in \mathbb{R}^3 \mid x^2 + y^2 < R^2; -b < z < b\} \quad (2)$$

where b is the cylinder half-length and R its radius.

One pore was carved from the centre of the cell and a quarter of a pore from each of its corners, giving a total of two in each simulation cell (Fig. 1b). Silicon atoms with incomplete valency (i.e. those not in a tetrahedral oxygen environment) as well as any oxygens bonded only to these silicons, were removed in a procedure similar to that used by Coasne et al. [35] This was followed by a 2000 time step MD relaxation in the NVT ensemble at 1 K (Fig. 1c), necessary to allow relaxation of the high energy surfaces created by the pore construction method.

The third stage of the MCM-41 construction process modifies the newly created pore surfaces. Hydrogen atoms were added until the required concentration of surface silanols was established. This was accomplished by placing hydrogen atoms a distance of 1.0 Å away from the centre of any non-bridging surface oxygens (defined to be those having fewer than two silicon atoms within a sphere of radius 2.3 Å centred on them) directed towards the centre of the pore (Fig. 1d). Fig. 2 shows a periodic representation of this cell, which reproduces the hexagonal mesoporous framework of MCM-41.

Two sets of models were constructed; one set of twelve models in which the wall thickness was kept constant and the pore diameter was varied (by carving different sized pores from each of the quenched amorphous silica configurations), and another set of five models in which the pore diameter was kept constant and the wall thickness was varied (by carving the same size pore from each of the five smallest simulation cells). The approach allowed us to easily and systematically vary the pore diameters from 2.4 to 5.9 nm and wall thicknesses from 0.95 to 1.76 nm. To enable comparison of the curved pore surface of MCM-41 with a flat surface (used to mimic MCM-41 in the large pore limit, which would otherwise require a very large simulation cell) a slit-pore model was constructed. This was prepared in a 3-step process similar to that used for the MCM-41 models but a rectangular slab of atoms

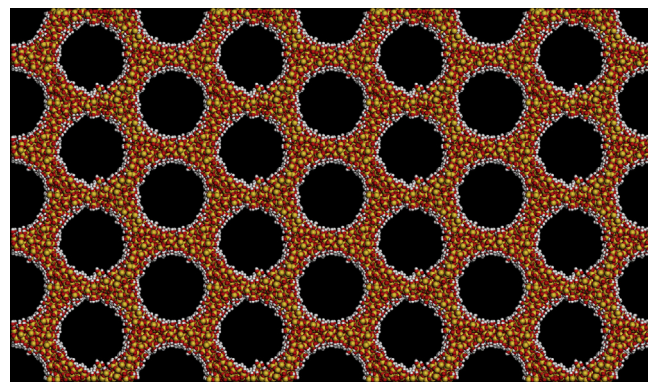


Fig. 2. The periodic hexagonal mesoporous framework of MCM-41, generated by replicating the model four times in each of the x and y direction. Colour scheme as for Fig. 1.

was removed instead of a cylinder. The slit-pore model created in this way had a pore width of 3.5 nm.

The internal surface area and free volume of each model were estimated using the Connolly method [36] as implemented in Materials Studio [37]. A spherical probe molecule with a radius of 1.84 Å was chosen to match the experimental surface areas typically obtained by applying the Brunauer-Emmett-Teller (BET) analysis [38] to N_2 adsorption isotherms. Estimates of the pore diameter and wall thickness were then obtained from the calculated internal volume using simple geometric relations for a cylinder.

2.2. Grand canonical Monte Carlo adsorption simulations

Adsorption isotherms in MCM-41 were constructed using the GCMC approach. In this method, four different ‘moves’ are attempted: molecules may be randomly inserted and deleted, as well as being translated and (for molecules possessing internal structure) rotated, by respective random linear and angular displacements. Moves were attempted with a probability of 0.2 for translations, 0.2 for rotations and 0.6 for insertions/deletions. These attempted moves were accepted with probability:

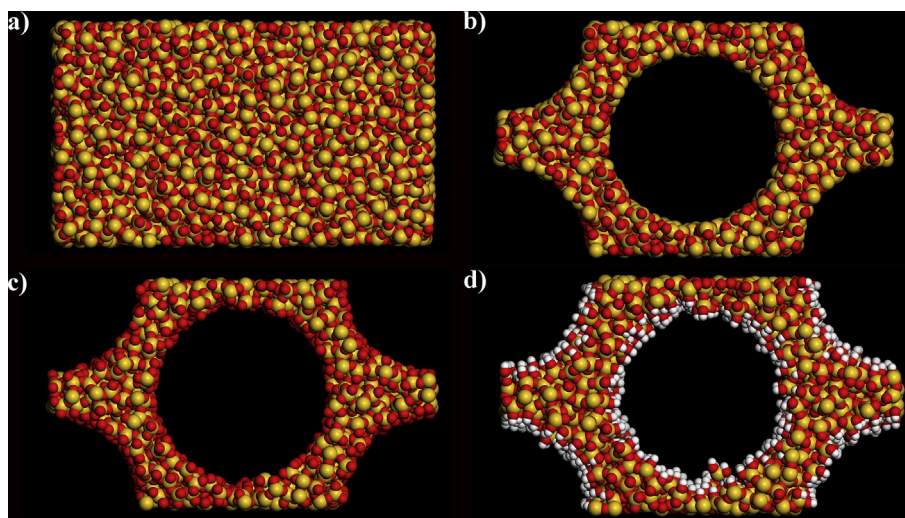


Fig. 1. The sequence of steps in the preparation of the MCM-41 models; a) quenched silica, b) carving of cylindrical pores, c) relaxation after removal of silicon and oxygen atoms on the pore surface and d) addition of hydrogen atoms to non-bridging oxygens. Yellow, red and white atoms are silicon, oxygen and hydrogen, respectively. (For interpretation of the references to colour in this figure legend, the reader is referred to the web version of this article.)

$$P^{acc} = \min\{1, \psi \exp(-\beta\Delta U)\} \quad (3)$$

where $\beta = 1/k_B T$, ΔU is the change in potential energy between the old state and the new state. The factor ψ is either $1, zV/(N+1)$ or $N/(zV)$ depending on whether the move is a translation/rotation, particle insertion or particle deletion, respectively. V is the volume, N the number of particles and z the activity of the adsorbate. The maximum linear and angular displacements were re-adjusted every 200 accepted moves in order to maintain acceptance ratios of 0.37. In our simulations a rigid (frozen atom) adsorbent model is used so only the adsorbate molecules undergo Monte Carlo moves.

A single GCMC run yields one point on an isotherm. Full isotherms are obtained by repeating the GCMC procedure for a series of different fugacities at a given temperature. Fugacity, f , is a more convenient choice of independent variable than activity; the two quantities being related by

$$\beta f = z \quad (4)$$

All of our GCMC simulations were performed using the DL_MONTE code [39]. Each simulation consisted of an initial run comprising 10 million attempted MC moves followed by a production run of 40 million attempted moves from which the statistics were collected, including the average number of molecules present within the pores of the adsorbent. This approach yields the absolute number of adsorbate molecules adsorbed in the material rather than the excess number as is commonly reported in experimental adsorption isotherms [40]. However, the difference between these two will be negligible in the Henry law (low pressure) region that we are primarily interested in here. All of the GCMC simulations were carried out at a temperature of 265 K for consistency with available experimental data.

Interactions between adsorbate–adsorbate and adsorbate–adsorbent atoms were modelled using a pair potential consisting of a Lennard-Jones plus Coulombic term:

$$\phi_{LJ}(r_{ij}) = \frac{q_i q_j}{4\pi\epsilon_0 r_{ij}} + 4\epsilon_{ij} \left[\left(\frac{\sigma_{ij}}{r_{ij}} \right)^{12} - \left(\frac{\sigma_{ij}}{r_{ij}} \right)^6 \right] \quad (5)$$

Site-specific parameters (σ_i , ϵ_i and q_i) are given for CO₂ (Table 2) and the adsorbent (Table 3). Cross-terms ϵ_{ij} and σ_{ij} were then obtained using Lorentz-Berthelot combining rules:

$$\epsilon_{ij} = \sqrt{\epsilon_i \epsilon_j}; \quad \sigma_{ij} = \frac{1}{2}(\sigma_i + \sigma_j) \quad (6)$$

The potential energy of each configuration was evaluated by summing over all pairs, including pairs of atoms on different adsorbent molecules and between atoms of an adsorbate molecule and an atom of the MCM-41 matrix. Initially, the amorphous silica parameters were taken from Brodka et al. [41] where bridging, O^b, and non-bridging (i.e. those on the surface), O^{nb}, oxygen atoms take different van der Waals diameters. A single ϵ_O parameter for both types of oxygen was optimised to improve agreement with the experimental CO₂ adsorption isotherm at pressures less than 1 atm. The dispersion of Si and H can be considered negligible in these materials so these elements are represented only with partial charges in the model. To maintain an electrically neutral simulation

Table 2
CO₂ parameters used in GCMC adsorption simulations [42].

	σ_i (Å)	ϵ_i/k_B (K)	q_i (e)
C	2.800	27.0	+0.700
O	3.050	79.0	−0.350

Table 3
Optimised parameters for MCM-41 atoms used in the MC simulations [41].

	σ_i (Å)	ϵ_i/k_B (K)	q_i (e)
O ^b	2.70	300.0	−0.629
O ^{nb}	3.00	300.0	−0.533
Si	—	—	1.256–1.277
H	—	—	0.206

cell q_{Si} was adjusted for each model. Si was chosen as our variable charge since adsorption is expected to be less sensitive to changes in the charge of Si than those of either O or H.

Experimental adsorption isotherms are usually plotted against pressure rather than fugacity. To facilitate comparison between model and experiment, we therefore converted the fugacity values into pressures using the Peng–Robinson equation of state [43].

$$P = \frac{RT}{v-b} - \frac{a(T)}{v(v+b) + b(v-b)} \quad (7)$$

in which R is the universal gas constant, $a(T)$ and b are the (temperature dependent) attraction parameter and van der Waals co-volume respectively, while v is the molar volume. The van der Waals parameters can be expressed in terms of the critical constants for the adsorbate, T_c , P_c and acentric factor, ω , by

$$b = 0.07780 \frac{RT_c}{P_c} \quad (8)$$

$$a(T) = a(T_c) \left[1 + \kappa \left(1 - \sqrt{T_r} \right) \right]^2 \quad (9)$$

$$a(T_c) = 0.45724 \left(\frac{R^2 T_c^2}{P_c} \right) \quad (10)$$

$$\kappa = 0.37464 + 1.54226\omega - 0.26992\omega^2 \quad (11)$$

where T_r is the relative temperature, T/T_c . The fugacity can then be calculated from

$$\ln\left(\frac{f}{p}\right) = (Z-1) - \ln(Z-B) - \frac{A}{2\sqrt{2}B} \ln\left[\frac{Z + (\sqrt{2}+1)B}{Z - (\sqrt{2}-1)B}\right] \quad (12)$$

where, $Z = \frac{Pv}{RT}$, $A = \frac{ap}{R^2 T^2}$, $b = \frac{bP}{RT}$.

For CO₂, we have used the following critical properties: $T_c = 304.1$ K and $P_c = 7.3825$ MPa and an acentric factor, $\omega = 0.239$ [44].

2.3. Zero coverage Monte Carlo simulations

The low pressure region of the adsorption isotherm is highly sensitive to the potential energy landscape of the adsorbent. Models with different pore widths, wall thicknesses and with different energy surfaces are best compared in this regime. A useful and computationally inexpensive tool (compared to GCMC) for this purpose is the so-called zero coverage MC method.

Zero coverage MC involves randomly placing a test molecule within the pore space of the adsorbent at a random orientation and computing the energy it experiences as a result of its interaction with the matrix. This potential energy and the Boltzmann factor are ensemble averaged over a sequence of several million test insertions, yielding two important thermodynamic quantities: the

zero-coverage heat of adsorption, q_{st}^0 , and the Henry law coefficient, K_H , respectively. The isosteric heat of adsorption is defined as the total heat release upon transferring a single adsorbate molecule from the bulk fluid phase to the adsorbed phase. For materials with a heterogeneous surface, such as MCM-41, the isosteric heat decreases rapidly as a function of adsorbate loading from its initially large value at zero coverage (q_{st}^0) as the most attractive surface sites become occupied with adsorbate atoms or molecules. K_H is the proportionality constant between the number of species adsorbed to the surface and the pressure.

The zero coverage heat of adsorption is evaluated from [20].

$$q_{st}^0 = k_B T - \langle U \rangle \quad (13)$$

where U is the total potential energy of interaction between the test particle and the adsorbent. K_H is determined using the relation [20].

$$K_H = \frac{\beta \langle \exp(-\beta U) \rangle}{A} \quad (14)$$

where A is the surface area of the adsorbent. In order to compare our values with those typically reported in experiments K_H was multiplied by the volume of the model system.

In this study we have conducted zero coverage runs using four different probe molecules: Ar, Kr, N₂, and CO₂. This set was chosen to enable the investigation of the adsorption of molecules with varying degrees of sensitivity to the charge distribution of the MCM-41 surface. Ar and Kr are expected to be fairly insensitive to this property compared with N₂ and CO₂. Where possible, we have also compared with published experimental data. The surface of MCM-41 has an important charge distribution, due to its heterogeneous nature and a high concentration of surface silanol groups. It has been shown previously that an adsorbate model with a charge distribution is required for the accurate prediction of adsorption behaviour of N₂ in MCM-41, particularly at low pressure [45].

The three-site TraPPE models of N₂ and CO₂ were used [42]. These rigid models have bond distances of 1.10 and 1.16 Å respectively. These models are known to accurately predict the phase behaviour and quadrupole moments of the gas molecules. Ar and Kr were modelled as single Lennard-Jones sites [46]. All interactions were calculated assuming a Lennard-Jones plus Coulombic function (Equations (5) and (6)). The parameters used for the N₂, Ar and Kr are given in Table 4. Those for CO₂ are the same as used in the GCMC simulations and can be found in Table 2. For all MC calculations cubic periodic boundary conditions were employed and the interaction potential terms were spherically truncated at 15 Å.

The Ewald summation is the most expensive part of the calculation. To make it more feasible, the electrostatic potential was pre-tabulated on a grid; the potential energy was then determined by 3D linear interpolation from the surrounding cube of tabulated points. A grid resolution of 0.2 Å was found to give errors in q_{st}^0 of less than 0.2 kJ mol⁻¹, relative to a simulation in which the Ewald sum was evaluated at each new configuration (without a grid).

Table 4

Parameters used in Monte Carlo zero coverage simulations [42,46]. N_q corresponds to the position of the remaining charge site at the centre of mass the TraPPE model.

	σ_i (Å)	ϵ_i/k_B (K)	q_i (e)
Ar	3.405	119.8	–
Kr	3.636	166.4	–
N	3.310	36.0	–0.482
N_q	–	–	+0.964

Zero coverage runs were performed at a temperature of 298 K. Between 10⁸ and 10¹⁰ MC moves were required to converge a single isosteric heat calculation (the criterion for convergence being no further change greater than order 10⁻³ kJ mol⁻¹ over 10⁷ random insertions). Due to the amorphous nature of the material it is possible for the test particle to be randomly inserted into energetically favourable yet physically inaccessible locations. To avoid this being incorporated into the Boltzmann weighted average we immediately reject any MC move that results in an adsorbate position in which the local density of the host (within a sphere with a radius of 5 Å) is representative of bulk amorphous silica. The rejection criterion was defined as the minimum value in the oxygen atom number density profile for the bulk material (57.3 atoms nm⁻³).

The effect of preparation quench rate, pore diameter and wall thickness on q_{st}^0 and K_H were investigated.

3. Results

3.1. MCM-41 model structure

The pair distribution function for oxygen atoms, $g_{O-O}(r)$, in the silica melt at 7300 K are compared to those obtained after quenching the silica to 300 K (Fig. 3). In the melt $g_{O-O}(r)$ shows a broad peak at 2.6 Å. The quenched silica has a more intense peak at this position as well as a significant secondary peak at 5 Å. As the quench rate is decreased these peaks converge, becoming more intense. The minimum at 3 Å present in the slower quenches is not present in the 7000 K ps⁻¹ quench rate. This quench rate therefore retains some structural characteristics of the melt. There is little difference in the structure of the 10 K ps⁻¹ quench rate model and the slowest quench rate (1 K ps⁻¹) so 10 K ps⁻¹ was considered as an acceptable rate for the preparation of our models.

By taking an average over 100 different samples, Zhuravlev [12] concluded that amorphous silica surfaces have a silanol density of 4.9 OH nm⁻². This is significantly higher than the density calculated by some other workers (e.g. Zhao et al., 3.0 OH nm⁻²) [10]. The wide range reported for amorphous silicas in the experimental literature reflects the different morphologies of samples and experimental conditions of preparation. The surfaces of the amorphous silica models in this work were heterogeneous and consisted of a combination of Q¹ (SiO(OH)₃), Q² (SiO₂(OH)₂), Q³ (SiO₃(OH)) and Q⁴ (siloxane) groups. Our MCM-41 models have a silanol density of 6.17 OH nm⁻², averaged over both the varying pore diameter and

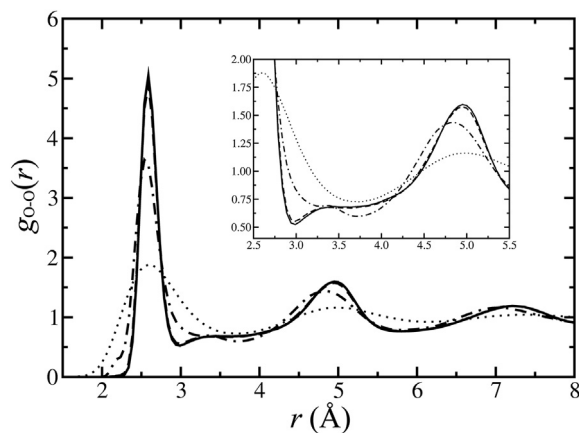


Fig. 3. $g_{O-O}(r)$ obtained after quenching from 7300 to 300 K at rates of 1 (solid line), 10 (dashes), and 7000 (dots/dashes) K ps⁻¹ and for the silica melt at 7300 K (dots). Inset: expanded region between 2.5 and 6.0 Å.

wall thickness sets of models. The density increases with increased curvature of the pore surface, from 5.9 OH nm⁻² for the largest pore (5.90 nm) to 7.0 OH nm⁻² for the narrowest (2.41 nm) in the series of models in which pore diameter is varied. These densities are in good agreement with those reported experimentally for MCM-41 and the related MCM-48 [13]. There is no evidence that preparing models at a slower quench rate leads to any significant change in silanol density.

3.2. Simulated GCMC isotherms

The simulated adsorption isotherm (Fig. 4) has a capillary condensation step at intermediate pressure, characteristic of mesoporous materials, and is classified as Type IV according to the IUPAC classification [47]. A number of different values for ϵ_0 have been proposed in the literature [48], in part due to the large variation in wall thicknesses and surface silanol densities of the real material against which parameters are optimized. The final value for ϵ_0/k_B used in these simulations was 300 K. Although the pressure at which capillary condensation occurs was slightly underestimated, there was extremely good agreement between the simulated and experimental isotherms at low pressure ($P < 1$ atm); *i.e.* the region most sensitive to the adsorbent-adsorbate potential.

The agreement between simulation and experiment indicates that this MCM-41 model is likely to have both a similar pore diameter and wall thickness to the experimental sample. The final configurations of adsorbate molecules in the isotherm simulations corresponding to the labels in Fig. 4a are shown in Fig. 5. The isotherms in Fig. 4a–c correspond to a model with a mean pore diameter and wall thickness of 3.16 and 0.95 nm respectively for a) the full range of pressures investigated, b) at low pressure and c) and in the Henry law region. The configurations in Fig. 5 show the gradual filling of the pore as a function of pressure. This occurs in four stages: a) adsorption of the first few CO₂ molecules prior to monolayer formation, b) monolayer formation, c) multilayer formation and d) as the pore approaches its maximum CO₂ capacity after capillary condensation.

The maximum CO₂ capacity of a material with these dimensions is predicted to be 13.9 mmol g⁻¹ from the high pressure region of the isotherm. The calculated surface area and pore volume of this model were 1010 m² g⁻¹ and 0.56 cm³ g⁻¹, respectively. The surface area falls well within the wide range reported in the literature, typically between 950 and 1250 m² g⁻¹. However the pore volume is less than that determined experimentally (approx. 0.80 cm³ g⁻¹). Since this property is strongly dependent on the dimensions of the adsorbate molecule, the discrepancy may be due to the unrealistic spherical approximation of the probe used in these calculations.

Fig. 6 shows the simulated adsorption isotherms for CO₂ in MCM-41 with pore diameters ranging from 2.41 to 3.85 nm and a constant wall thickness of 0.95 nm. The maximum CO₂ capacities of these models range from 11.1 to 16.7 mmol g⁻¹ and the capillary condensation step occurs at higher pressures and becomes more distinctive as the pore diameter increases. At low and intermediate pressures adsorption is greatest for the models with the smallest pore diameter and the greatest surface silanol density.

3.3. Adsorption at zero coverage

We have investigated the variation of isosteric heat with the models prepared at different quench rates but all with approximately the same pore diameter (3.16 nm) and wall thickness (0.95 nm) as the one used to generate the isotherm in Fig. 4. Fig. 7 shows that for very fast quench rates q_{st}^0 fluctuates and this is more pronounced for adsorbate molecules with a larger q_{st}^0 such as CO₂. The fluctuations result from rapid quench rates generating an

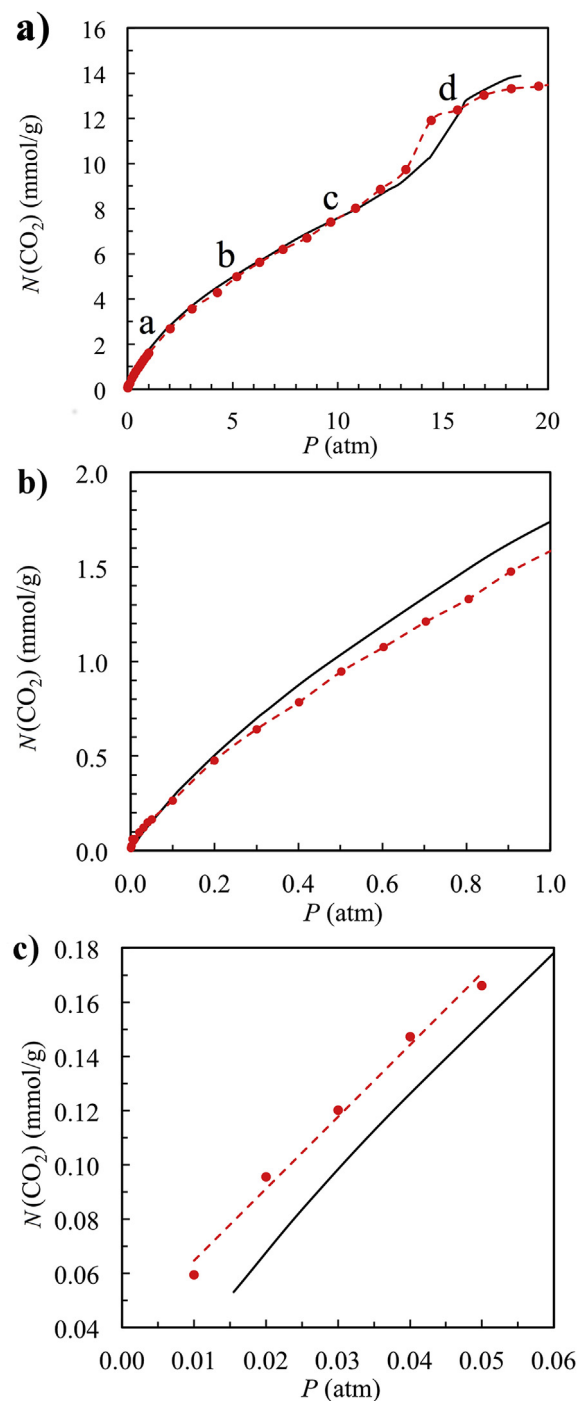


Fig. 4. Isotherm for CO₂ adsorption to MCM-41 with a pore diameter of 3.16 nm at 265 K for a) the full pressure range, b) the low pressure region and c) the Henry law region. The solid black line is the experimental data [49] and the red circles indicate the simulated data. The red dashed line through the simulated data is a guide to the eye in a) and b) and a line of best fit is used to estimate K_H in c). (For interpretation of the references to colour in this figure legend, the reader is referred to the web version of this article.)

unrealistic configuration of atoms on the surface of the metastable MCM-41. As the quench rate is decreased q_{st}^0 starts to converge, however a compromise must be reached between obtaining a realistic structure and the speed at which the MCM-41 models can be prepared. In this work 10 K ps⁻¹ was found to be an acceptable compromise and the results reported herein are for models prepared at this quench rate.

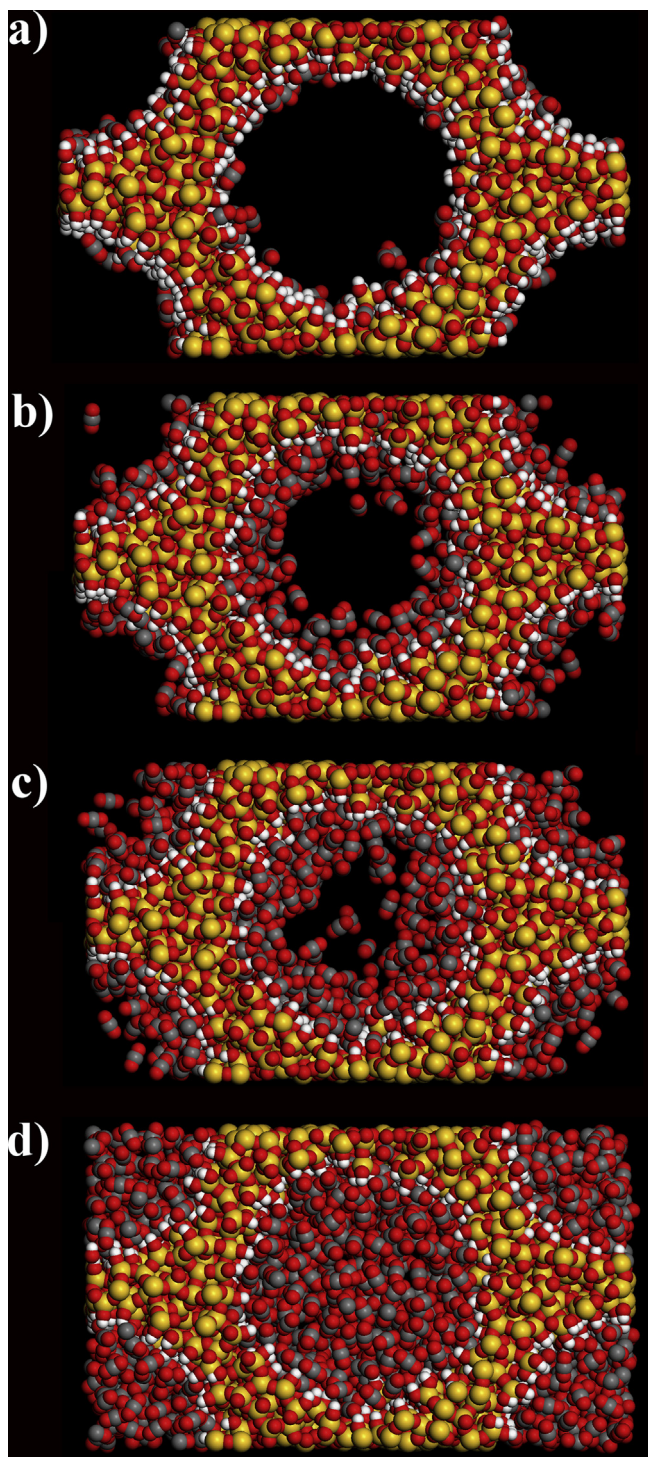


Fig. 5. Final configurations of GCMC simulations for CO₂ adsorbed to MCM-41 at pressures: a) before monolayer formation (1 atm), b) when a monolayer forms (5 atm), c) when multilayers form before capillary condensation (10 atm) and d) when the pore approaches its maximum capacity (15 atm).

The values q_{st}^0 and K_H for each adsorbate species, averaged over all pore diameters at a constant wall thickness, are given in Table 5. The average for CO₂ is much larger than for N₂, Ar and Kr and demonstrates that at very low pressures CO₂ preferentially adsorbs to MCM-41 over these other gases. Although it is straightforward to determine q_{st}^0 from molecular simulation, it is challenging to access low enough concentrations for its accurate experimental

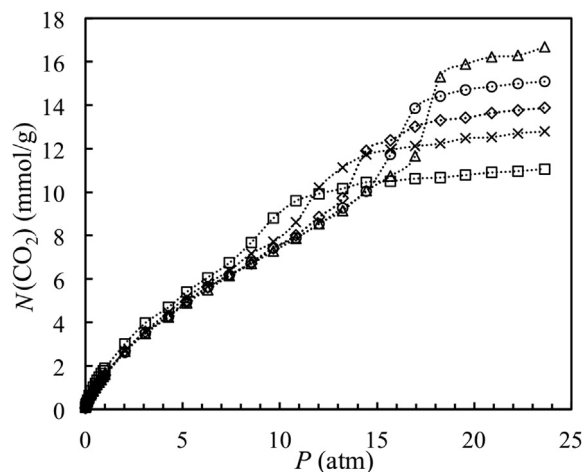


Fig. 6. Simulated adsorption isotherms for CO₂ in MCM-41 with pore diameters of 2.41 (squares), 2.81 (crosses), 3.16 (diamonds), 3.50 (circles) and 3.85 (triangles) nm.

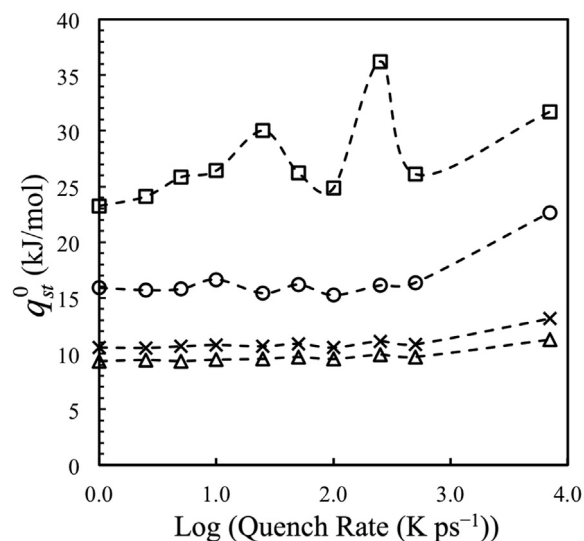


Fig. 7. The convergence of q_{st}^0 with decreasing quench rate for CO₂ (squares), Kr (circles), Ar (crosses) and N₂ (triangles) in MCM-41. The dashed lines are added as a guide to the eye.

determination. Simulations have shown that the isosteric heat of adsorption initially decreases very rapidly as adsorption loading increases [35,48]. As a result, the calculated values of q_{st}^0 might not be directly comparable with the experimental data at higher concentration. Furthermore, there is significant variability between reported experimental data for the same molecule (e.g. for CO₂, $q_{st}^0 = 20 \text{ kJ mol}^{-1}$ and 32 kJ mol^{-1}) [50,51], reflecting differences in the specific configuration of atoms on the surface of the MCM-41 pore. In our calculations, the average q_{st}^0 for CO₂ was

Table 5
 q_{st}^0 and K_H in MCM-41, averaged over 12 models with a pore wall thickness of 0.95 nm, with pore diameters ranging from 2.41 to 5.90 nm.

Adsorbate	q_{st}^0 (kJ mol ⁻¹)		K_H (mmol g ⁻¹ atm ⁻¹)
	This work	Experiment [7,50–53]	
CO ₂	26.5	20–32	0.93
N ₂	9.1	–	0.10
Ar	10.5	11–13	0.12
Kr	16.4	15	0.31

26.5 kJ mol⁻¹, falling within the range of experimentally reported values, whereas for Ar, q_{st}^0 is slightly lower than the experimental value. The slight under-prediction may be due to the fact that the real material may have some surface irregularities and exposed Si or O atoms (without silanols) that would result in an increase in q_{st}^0 . Such irregularities are thought to be uncommon on the surface of MCM-41, so much larger models are required to incorporate them at a realistic concentration.

A separate calculation was performed to determine K_H for CO₂ at 265 K to enable comparison with a value obtained from the linear, vanishing pressure part of the isotherm, in the Henry law region (less than 0.05 atm) of the CO₂ adsorption isotherm in Fig. 4c. Approximate agreement was found between the two approaches; $K_H = 2.81 \text{ mmol g}^{-1} \text{ atm}^{-1}$ from Equation (14) compared to $2.65 \text{ mmol g}^{-1} \text{ atm}^{-1}$ from the isotherm in Fig. 4c. The difference is due to significant statistical uncertainties in the adsorbed number of particles at very low pressure in the GCMC isotherms. The larger value of K_H at 265 K than 298 K is due to the fact that more gas molecules become adsorbed because they lack sufficient kinetic energy to escape the potential well of the adsorbent surface.

The variation in q_{st}^0 and K_H with pore diameter for a given wall thickness (0.9 nm) was investigated (Fig. 8). For adsorbates with a small q_{st}^0 there is a trend of increasing q_{st}^0 for smaller pore diameters, which has been observed previously during experimental studies of N₂ and Ar adsorption [7]. This geometrical effect is due to the increased curvature (and higher density of silanols) of the surface for narrower pore MCM-41 and is most pronounced in the case of N₂, where q_{st}^0 increases from 8.4 kJ mol⁻¹ to 10.6 kJ mol⁻¹ as the pore diameter decreases from 5.9 nm to 2.4 nm. For adsorbates with a larger q_{st}^0 (Kr and CO₂) this trend is obscured by larger fluctuations in q_{st}^0 as they are much more sensitive to the surface heterogeneity and the specific configuration of atoms at the surface. The observed fluctuations are not due to poor sampling (q_{st}^0 was converged to within 10⁻³ kJ mol⁻¹ over 10⁷ random insertions) but pores that are too short to incorporate all possible types of adsorption site. They could be dampened either by constructing models with much longer pores, or by taking an average value of q_{st}^0 over many models with the same diameter pore. Since all of the results for CO₂ are within the range reported experimentally, we have deemed this step unnecessary, but predict that such a

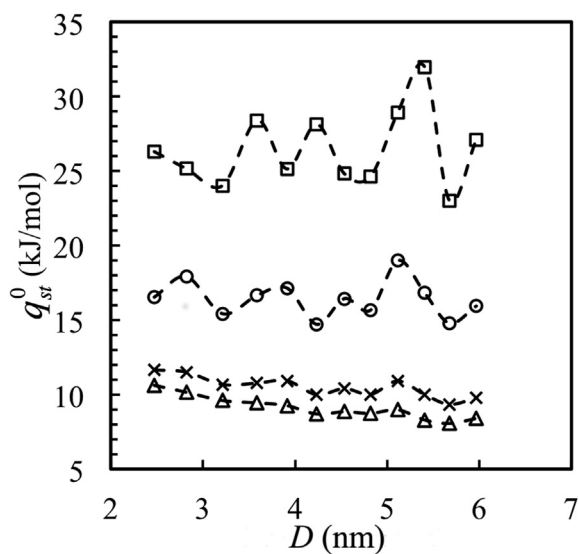


Fig. 8. The relationship between q_{st}^0 and pore diameter, D , for the four adsorbate species studied; CO₂ (squares), Kr (circles), Ar (crosses) and N₂ (triangles), at 298 K in a MCM-41 model with pore walls of 0.95 nm thickness.

procedure would be likely to reveal the same dependence on pore diameter as the other adsorbate molecules. No trend was observed for K_H in models with different pore diameters for any of the adsorbates studied.

The isosteric heats calculated for CO₂ and N₂ in the slit pore were 23.7 and 6.8 kJ mol⁻¹, respectively. This is much lower than the average value for the MCM-41 models and is likely to be due to the lower density of silanols on a flat surface (5.0 OH groups nm⁻²) compared to MCM-41 (5.9–7.0 OH groups nm⁻²). For the spherical adsorbates, q_{st}^0 did not decrease for Ar (11.5 kJ mol⁻¹) and Kr (18.4 kJ mol⁻¹) in the slit pore compared with MCM-41 and are therefore insensitive to the decrease in silanol density.

MCM-41 materials with thick pore walls are known to have greater thermal and hydrothermal stability than those with thin walls [8]. No trend in q_{st}^0 was observed with increasing wall thickness in the set of five models with a constant pore diameter. However, in contrast to its pore diameter independence, K_H decreases rapidly from a model with 0.95 nm (1.042 mmol g⁻¹ atm⁻¹) to 1.76 nm (0.480 mmol g⁻¹ atm⁻¹) thick walls. Although the total internal surface areas of these models are roughly similar, the difference is a result of the decreasing surface area per mass unit of the material, decreasing from 1018 m² g⁻¹ for 0.95 nm walls to 428 m² g⁻¹ for 1.76 nm walls.

4. Conclusions

This research demonstrates the ability of molecular simulation to optimize the physical adsorption process at very low pressure by modifying structural parameters. The approach by which the MCM-41 model structures were constructed enables easy alteration of the pore diameter and wall thickness. Validation of the model structure at very low pressure is advantageous because this is the region most sensitive to the adsorbent potential. In general, our findings predict that optimum adsorption of simple gas species to MCM-41 materials (large q_{st}^0 and K_H) at low pressure can be achieved with narrow pore diameters in agreement with experiment [7], although this trend is not obvious for adsorbates with a large q_{st}^0 (CO₂ and Kr). An improved model could be built with a slower and more realistic quench rate, but this would require a simulation timescale inaccessible to conventional molecular simulation techniques. However, preparation quench rates of less than 10 K ps⁻¹ result in models that accurately predict the extent of CO₂ adsorption and isosteric heat (26.5 kJ mol⁻¹) in the Henry law region. Henry law constants for CO₂ at 298 K were predicted using two approaches; firstly by determining the gradient of the adsorption isotherm at pressures less than 0.1 atm and secondly using Equation (14), involving a simulation with a single adsorbate molecule that was allowed to make a free and unhindered exploration of the adsorbent model surface. These two methods were in good agreement resulting in Henry law constants of 2.65 and 2.81 mmol g⁻¹ atm⁻¹, respectively. Improvements could be found by accounting more accurately for adsorbate-adsorbent interactions by abandoning the simple Lennard-Jones 12-6 potential and instead adopting a more complex form that includes induction such as the PN-TrAZ potential [54].

Supporting information

The output data from the simulations used in Figs. 4 and 6–8 and the atomic coordinates of the MCM-41 model used to generate the adsorption isotherms in Fig. 4 are available free of charge via the Internet at <http://pubs.acs.org>.

Notes

The authors declare no competing financial interest.

Acknowledgement

Funding Sources: We thank the EPSRC EP/G0371401/1 and the Nuclear FIRST Centre for Doctoral Training for funding this research and the University of Manchester for use of the Computational Shared Facility.

Experimental Data: We thank Yufeng He and Tina Düren for providing the experimental CO₂ adsorption isotherm data.

Appendix A. Supplementary data

Supplementary data related to this article can be found at <http://dx.doi.org/10.1016/j.micromeso.2016.03.034>.

References

- [1] C.T. Kresge, M.E. Leonowicz, W.J. Roth, J.C. Vartuli, J.S. Beck, Ordered mesoporous molecular-sieves synthesized by a liquid-crystal template mechanism, *Nature* 359 (6397) (1992) 710–712.
- [2] J.S. Beck, J.C. Vartuli, W.J. Roth, M.E. Leonowicz, C.T. Kresge, K.D. Schmitt, C.T.W. Chu, D.H. Olson, E.W. Sheppard, S.B. McCullen, J.B. Higgins, J.L. Schlenker, A new family of mesoporous molecular-sieves prepared with liquid-crystal templates, *J. Am. Chem. Soc.* 114 (27) (1992) 10834–10843.
- [3] P.I. Ravikovich, A. Vishnyakov, A.V. Neimark, M. Carrott, P.A. Russo, P.J. Carrott, Characterization of micro-mesoporous materials from nitrogen and toluene adsorption: experiment and modeling, *Langmuir* 22 (2) (2006) 513–516.
- [4] C.G. Sonwane, S.K. Bhatia, Characterization of pore size distributions of mesoporous materials from adsorption isotherms, *J. Phys. Chem. B* 104 (39) (2000) 9099–9110.
- [5] M. Carrott, A.J.E. Candeias, P.J.M. Carrott, P.I. Ravikovich, A.V. Neimark, A.D. Sequeira, Adsorption of nitrogen, neopentane, n-hexane, benzene and methanol for the evaluation of pore sizes in silica grades of MCM-41, *Micropor. Mesopor. Mat.* 47 (2–3) (2001) 323–337.
- [6] M. Kruk, M. Jaroniec, J.H. Kim, R. Ryoo, Characterization of highly ordered MCM-41 silicas using X-ray diffraction and nitrogen adsorption, *Langmuir* 15 (16) (1999) 5279–5284.
- [7] A.V. Neimark, P.I. Ravikovich, M. Grun, F. Schuth, K.K. Unger, Pore size analysis of MCM-41 type adsorbents by means of nitrogen and argon adsorption, *J. Colloid Interface Sci.* 207 (1) (1998) 159–169.
- [8] R. Mokaya, Improving the stability of mesoporous MCM-41 silica via thicker more highly condensed pore walls, *J. Phys. Chem. B* 103 (46) (1999) 10204–10208.
- [9] K. Cassiers, T. Linssen, M. Mathieu, M. Benjelloun, K. Schrijnemakers, P. Van Der Voort, P. Cool, E.F. Vansant, A detailed study of thermal, hydrothermal, and mechanical stabilities of a wide range of surfactant assembled mesoporous silicas, *Chem. Mater.* 14 (5) (2002) 2317–2324.
- [10] X.S. Zhao, G.Q. Lu, A.K. Whittaker, G.J. Millar, H.Y. Zhu, Comprehensive study of surface chemistry of MCM-41 using Si-29 CP/MAS NMR, FTIR, pyridine-TPD, and TGA, *J. Phys. Chem. B* 101 (33) (1997) 6525–6531.
- [11] A. Jentys, K. Kleestorfer, H. Vinek, Concentration of surface hydroxyl groups on MCM-41, *Micropor. Mesopor. Mat.* 27 (2–3) (1999) 321–328.
- [12] L.T. Zhuravlev, Concentration of hydroxyl-groups on the surface of amorphous silicas, *Langmuir* 3 (3) (1987) 316–318.
- [13] H. Landmesser, H. Kosslick, W. Storek, R. Fricke, Interior surface hydroxyl groups in ordered mesoporous silicates, *Solid State Ionics* 101 (1997) 271–277.
- [14] X.C. Xu, C.S. Song, J.M. Andresen, B.G. Miller, A.W. Scaroni, Preparation and characterization of novel CO₂ “molecular basket” adsorbents based on polymer-modified mesoporous molecular sieve MCM-41, *Micropor. Mesopor. Mat.* 62 (1–2) (2003) 29–45.
- [15] A. Corma, From microporous to mesoporous molecular sieve materials and their use in catalysis, *Chem. Rev.* 97 (6) (1997) 2373–2419.
- [16] G.E. Fryxell, J. Liu, S. Mattigod, Self-assembled monolayers on mesoporous supports (SAMMS) – an innovative environmental sorbent, *Mater. Technol.* 14 (4) (1999) 188–191.
- [17] R. Van der Vaart, C. Huiskes, H. Bosch, T. Reith, Single and mixed gas adsorption equilibria of carbon dioxide/methane on activated carbon, *Adsorpt. J. Int. Adsorpt. Soc.* 6 (4) (2000) 311–323.
- [18] B.P. Feuston, J.B. Higgins, Model structures for MCM-41 materials – a molecular dynamics simulation, *J. Phys. Chem.* 98 (16) (1994) 4459–4462.
- [19] M.W. Maddox, K.E. Gubbins, Molecular simulation of fluid adsorption in buckytubes and MCM-41, *Int. J. Thermophys.* 15 (6) (1994) 1115–1123.
- [20] W.A. Steele, *The Interactions of Gases with Solid Surfaces*, Pergamon Press, 1974.
- [21] M.W. Maddox, J.P. Olivier, K.E. Gubbins, Characterization of MCM-41 using molecular simulation: heterogeneity effects, *Langmuir* 13 (6) (1997) 1737–1745.
- [22] K. Kleestorfer, H. Vinek, A. Jentys, Structure simulation of MCM-41 type materials, *J. Mol. Catal. A Chem.* 166 (1) (2001) 53–57.
- [23] Y.F. He, N.A. Seaton, Experimental and computer simulation studies of the adsorption of ethane, carbon dioxide, and their binary mixtures in MCM-41, *Langmuir* 19 (24) (2003) 10132–10138.
- [24] F.R. Siperstein, K.E. Gubbins, Phase separation and liquid crystal self-assembly in surfactant-inorganic-solvent systems, *Langmuir* 19 (6) (2003) 2049–2057.
- [25] M. Jorge, J.R.B. Gomes, M. Natalia, D.S. Cordeiro, N.A. Seaton, Molecular simulation of silica/surfactant self-assembly in the synthesis of periodic mesoporous silicas, *J. Am. Chem. Soc.* 129 (50) (2007) 15414–15415.
- [26] M. Jorge, J.R.B. Gomes, M. Cordeiro, N.A. Seaton, Molecular dynamics simulation of the early stages of the synthesis of periodic mesoporous silica, *J. Phys. Chem. B* 113 (3) (2009) 708–718.
- [27] L. Jin, S.M. Auerbach, P.A. Monson, Simulating the formation of surfactant-templated mesoporous silica materials: a model with both surfactant self-assembly and silica polymerization, *Langmuir* 29 (2) (2013) 766–780.
- [28] C.G. Sonwane, C.W. Jones, P.J. Ludovice, A model for the structure of MCM-41 incorporating surface roughness, *J. Phys. Chem. B* 109 (49) (2005) 23395–23404.
- [29] B.W.H. Van Beest, G.J. Kramer, R.A. Van Santen, Force fields for silicas and aluminophosphates based on abinitio calculations, *Phys. Rev. Lett.* 64 (16) (1990) 1955–1958.
- [30] Y. Guissani, B. Guillot, A numerical investigation of the liquid-vapor coexistence curve of silica, *J. Chem. Phys.* 104 (19) (1996) 7633–7644.
- [31] M.F. Camellone, J. Reiner, U. Sennhauser, L. Schlappach, Efficient generation of realistic model systems of amorphous silica, *ArXiv* (2011) 1109–2852.
- [32] M.P. Allen, D.J. Tildesley, *Computer Simulation of Liquids*, Clarendon Press, Oxford, 1989.
- [33] W.G. Hoover, Canonical dynamics – equilibrium phase-space distributions, *Phys. Rev. A* 31 (3) (1985) 1695–1697.
- [34] S. Melchionna, G. Ciccotti, B.L. Holian, Hoover NPT dynamics for systems varying in shapes and size, *Mol. Phys.* 78 (3) (1993) 533–544.
- [35] B. Coasne, F.R. Hung, R.J.M. Pellenq, F.R. Siperstein, K.E. Gubbins, Adsorption of sample gases in MCM-41 materials: the role of surface roughness, *Langmuir* 22 (1) (2006) 194–202.
- [36] M.L. Connolly, Analytical molecular-surface calculation, *J. Appl. Crystallogr.* 16 (1983) 548–558.
- [37] A.S. Inc, *Materials Studio, Accelrys*, San Diego, CA, USA, 2001.
- [38] S. Brunauer, P.H. Emmett, E. Teller, Adsorption of gases in multimolecular layers, *J. Am. Chem. Soc.* 60 (1938) 309–319.
- [39] J.A. Purton, J.C. Crabtree, S.C. Parker, DL_MONTE: a general purpose program for parallel Monte Carlo simulation, *Mol. Simul.* 39 (14–15) (2013) 1240–1252.
- [40] D. Nicholson, N.G. Parsonage, *Computer Simulation and the Statistical Mechanics of Adsorption*, Academic Press, London, 1982.
- [41] A. Brodka, T.W. Zerd, Properties of liquid acetone in silica pores: molecular dynamics simulation, *J. Chem. Phys.* 104 (16) (1996) 6319–6326.
- [42] J.J. Potoff, J.I. Siepmann, Vapor-liquid equilibria of mixtures containing alkanes, carbon dioxide, and nitrogen, *AIChE J.* 47 (7) (2001) 1676–1682.
- [43] D. Peng, D.B. Robinson, New two-constant equation of state, *Industrial Eng. Chem. Fundam.* 15 (1) (1976) 59–64.
- [44] J.M. Prausnitz, R.N. Lichtenthaler, E.G. de Azevedo, *Molecular Thermodynamics of Fluid-phase Equilibria*, third ed., Prentice Hall, 1998.
- [45] B. Coasne, A. Galarneau, F. Di Renzo, R.J.M. Pellenq, Molecular simulation of nitrogen adsorption in nanoporous silica, *Langmuir* 26 (13) (2010) 10872–10881.
- [46] J.O. Hirschfelder, C.F. Curtiss, R.B. Bird, *Molecular Theory of Gases and Liquids*, Wiley, New York, 1964.
- [47] K.S.W. Sing, D.H. Everett, R.A.W. Haul, L. Moscou, R.A. Pierotti, J. Rouquerol, T. Siemieniowska, Reporting physisorption data for gas-solid systems with special reference to the determination of surface-area and porosity (recommendations 1984), *Pure Appl. Chem.* 57 (4) (1985) 603–619.
- [48] C. Herdes, C.A. Ferreiro-Rangel, T. Duren, Predicting neopentane isosteric enthalpy of adsorption at zero coverage in MCM-41, *Langmuir* 27 (11) (2011) 6738–6743.
- [49] Y.F. He, The Effect of Adsorbent Heterogeneity on Pure Gas and Multicomponent Adsorption Equilibrium Especially at Low Pressures, and Accurate Prediction of Adsorption Equilibrium, Ph.D. Thesis, University of Edinburgh, Edinburgh, UK, 2005.
- [50] T.C. dos Santos, S. Bourrelly, P.L. Llewellyn, J.W.D. Carneiro, C.M. Ronconi, Adsorption of CO₂ on amine-functionalised MCM-41: experimental and theoretical studies, *Phys. Chem. Chem. Phys.* 17 (16) (2015) 11095–11102.
- [51] M.R. Mello, D. Phanon, G.Q. Silveira, P.L. Llewellyn, C.M. Ronconi, Amine-modified MCM-41 mesoporous silica for carbon dioxide capture, *Micropor. Mesopor. Mat.* 143 (1) (2011) 174–179.
- [52] J.P. Olivier, in: G. Kreysa, J.P. Baselt, K.K. Unger (Eds.), *Studies in Surface Science and Catalysis: Characterisation of Porous Solids V*, Elsevier Science B.V., Amsterdam, The Netherlands, 2000, pp. 81–87.
- [53] J.P. Olivier, in: D.D. Do (Ed.), *Adsorption Science and Technology*, World Scientific Publishing Co. Pte. Ltd., Singapore, 2000, pp. 472–476.
- [54] R.J.M. Pellenq, D. Nicholson, Intermolecular potential function for the physical adsorption of rare-gases in silicalite, *J. Phys. Chem.* 98 (50) (1994) 13339–13349.